FEMTOSECOND LASER DRILLING OF SILICON NITRIDE

L. Marquez, S. Nevarez*, C. M. Stewart
The University of Texas at El Paso, El Paso Texas, 79968, USA; Department of Aerospace and Mechanical Engineering
*Corresponding Author (snevarez8@miners.utep.edu)

Keywords: Femtosecond laser ablation, Ceramics, Silicon Nitride, Characterization

Abstract

This research focuses on the laser drilling of deep zero-taper features in Silicon Nitride (Si_3N_4) ceramic. The goal is to develop laser parameters for the drilling zero-taper circular holes where the hole diameter is 4 mm and depth is 3 mm. In this work, the laser power percentage is increased from 50%, 60%, and 70% to evaluate the influence of the % power on the quality of drilled holes. Digital microscopy of the drilled holes is performed to measure and evaluate the inlet and outlet diameters, cylindricity, taper and taper angle. It is determined that as the % power increases, the inlet and outlet hole increases in diameter, and the shear lip decreases to a limit of 70% power. At an increased % power of 75.5%, cylindricity, taper and taper angle improve but at the expense of the inlet, outlet, and shear lip. This can be corrected by rescaling the part to achieve an exact diameter and surface polishing to remove the shear lip.

Introduction

Ceramics are employed in various engineering applications including electronics, semiconductors, automotive and aerospace industry, among others. Ceramics are desirable materials due to their high hardness, thermal resistance, chemical, thermal, and mechanical properties. A drawback of engineering ceramics is the manufacturing process. Ceramics are hard and brittle and conventional drilling or cutting methods can damage the material. These challenges in manufacturing have limited the application of ceramics in certain engineering applications [1]. The non-contact machining of ceramics through ultrashort pulsed laser drilling offers a possible solution to the manufacturing issues.

The advantage of laser drilling is the ability to machine hard and brittle materials. A laser, pulsed in the time regime of femtoseconds (fs), drills/machines sharp and well-defined holes and cuts [2]. Additionally, the short pulse width results in limited melting, cracking, or heat transfer to the surrounding material, as well as no residual stresses. This non-contact process can greatly aid in the machining of hard materials. This study focuses on drilling into silicon nitride to produce zero-taper through holes. With this, other thicknesses can be explored, to achieve zero-taper holes.

Objectives

The objective herein is to optimize the laser parameters of deep zero- taper through holes in Si_3N_4 and achieve a hole diameter of 4-mm, hole depth of 3 mm, and cylindricity, taper and taper angle near or equal to zero. Using a femtosecond laser system, Si_3N_4 plates are drilled over a range of laser power percentages (50, 60, 70%) with the remaining laser parameters fixed as control variables (repetition rate, repeat, hatch spacing, and scanning speed). A Keyence digital microscope is employed to characterize the drilled holes using measurement tools and 3D

mapping. It is hypothesized as % power increases; the quality of drilled holes (across all measurements) will improve. The increase in energy will result in discoloration and breakage.

Equipment/Materials

A 6DLaser femtosecond laser machining system consisting of an Edgewave laser, Scanlab Galvanometer scanner, and ALIO control system/software is employed in this study. The laserhead has a pulse duration of 600 fs, wavelength of 1030 nm, and average power ranging from 90-600 W depending on the repetition rate. The optics of the Galvo Scanner are tuned to provide a spot size of 20 μm at the target.

The subject material is Silicon Nitride (Si_3N_4) circular plates measuring 81-mm x 3-mm. The material composition is provided in Table 1. Silicon nitride is difficult to sinter because of the strong covalent bonding between Si and N atoms. Therefore, the additives, alumina and yttria, help in the densification of sintering Si_3N_4 [3].

Table 1: Material composition of Si_3N_4 [4]

Material Composition	(wt%)
Aluminum Oxide (Al_2O_3)	4
Silicon Nitride (Si_3N_4)	90
Yttria (Y_2O_3)	6

Machining: Conventional versus Laser

Key mechanical and thermal properties for conventional machinability are provided in Table 2 [4]. Conventional machining is unsuccessful on ceramics because the cutting action works on the principle of chip formation due to shearing and machining ceramics leads to breakage because of their brittleness [5]. It may cause damage to the cutting tool and ceramic.

Table 2: Material properties [4]

Mechanical	
Hardness (MPa)	8000-30500
Youngs Modulus (GPa)	166-297
Tensile Strength (MPa)	60-525
Compressive Strength (MPa)	524-5500
Thermal	
Thermal Conductivity (W/(m·K))	20
Melting Temperature (K)	2661-2769
Specific Heat (J/ (kg · K))	673-1100
Thermal Conductivity @ 20°C (W/ m·K)	20

Laser machining is driven by the physics of photon-matter interaction where a coherent beam of photons transmits heat energy into matter. Given a high enough energy density and rate of heat transfer the matter has the propensity vaporize/ablation (at low pulse widths i.e. pico and femtoseconds) or melt/fusion (high pulse widths, i.e. nanoseconds or greater) [6]. Wilson proposed a method for calculating the energy (in kJ) to vaporize a given mass, *m* (in kg) as follows

$$E_v = m\left[C_S(T_m - T) + C_L(T_v - T_m) + L_f + L_v\right] \quad (1)$$

where T is the initial Temperature, T_m is the melting temperature, T_v is the boiling temperature, C_S and C_L are the solid and liquid specific heat capacity respectively, and L_f and L_v are the latent heat of fusion and vaporization [7]. When the following conditions are true,

$$L_f \ll L_v, \qquad T \ll T_v, \qquad C_S \gg C_L = C \quad (2)$$

Then the energy calculation simplifies to

$$E_v = m(CT_v + L_v) \quad (3)$$

Conversely, a similar equation has been developed for calculating the energy deposited into a sample by laser machining as a function of the laser parameters [8]. Future work involves developing a formula for predicting not only the energy required to vaporize/ablation but also the required laser processing parameters. Nevertheless, in this study we take an empirical approach to improving the laser drilling parameters.

Characterization

A Keyence VHX-970F Digital Microscope with magnification ranging from 20x to 2000x is employed to evaluate the cylindricity, taper and taper angle of the drilled holes. The samples were cleaned using a Branson ultrasonic bath (3461K41, McMaster-Carr, CA, USA) for 20 minutes using a water-based cleaning solution before microscopy. The thickness is measured using calipers.

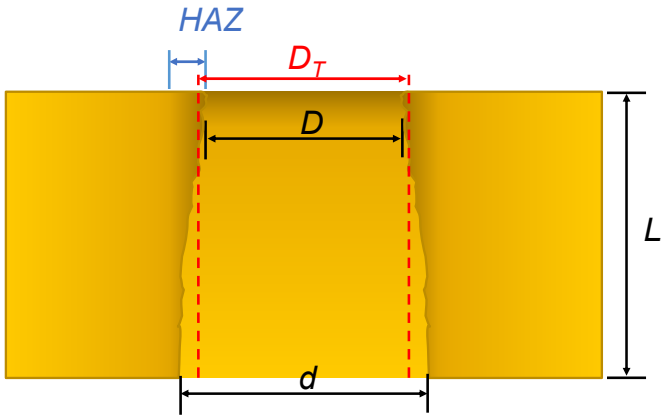

Figure 1: Taper dimension

Hole measurements are taken as illustrated in Figure 1. Measurements are taken of D the hole inlet diameter, d the hole outlet diameter, L the specimen thickness, HAZ the heat affected zone, and t_s the thickness of the crescent-shaped shear lip measured in the thickness location. The inlet and outlet diameters are measured by flipping the plate. A sequence of z-stack images (with the inlet side-up) are gathered to generate 3D maps and 2D images with a greater depth of field.

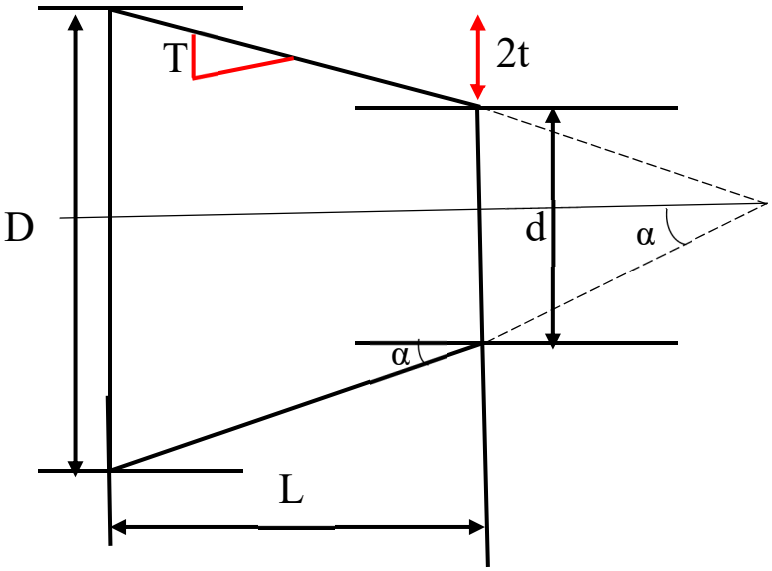

Figure 2: Taper angle calculation

Cylindricity is defined as a measure of how close to "true" a cylindrical feature is and employed to ensure roundness and straightness along the neutral axis [9]. The simplest measure of cylindricity, *t* is calculated as

$$t = (D - d) \tag{1}$$

where when the inlet and outlet hole diameters are 4 mm, the cylindricity is zero. Taper, *T,* is defined as the decrease in hole diameter with increasing depth (i.e., the slope of the hole wall) it is calculated as follows [10]

$$T = (D\text{-}d)/L \tag{2}$$

where when cylindricity is zero, the taper is zero. Taper angle, α, is the angle calculated from taper as shown in Figure 2, it is calculated as follows

$$\alpha = \tan^{-1}\left(\frac{D - d}{2L}\right) \tag{3}$$

where *D* is the diameter of the hole at the top, *d* is the diameter of the hole at the bottom and *L* is the height of the sample [11].

Note, the given cylindricity, taper, and taper angle calculations are of the simplest form which considers only measurements at the inlet and outlet. More detailed measures of taper and cylindricity through-thickness can be obtained by processing the 3D mapping data. Such measures are future work.

Experimental Design

Drilling operations were performed at the power percentages ranging from 50-70% and hatch spacing of 0.015. The test matrix completed for a hatch spacing of 0.015 mm, as provided in Table 3. All other parameters were fixed as control variables. Based on the results of the first test matrix,

a secondary test was performed at a power percentage of 75.5% as highlighted in grey within Table 3.

Table 3: Laser parameters at spacing of 0.015 mm

Parameters	L50	L60	L70	L75.5
Power (%)	50	60	70	75.5
Power from graph (W)	52.04	62.448	72.856	78.58
Rep. rate (kHz)	500	500	500	500
Scanning Speed (mm/s)	100	100	100	100
Hatch Type	contour	contour	contour	contour
Hatch Spacing (mm)	0.015	0.015	0.015	0.015

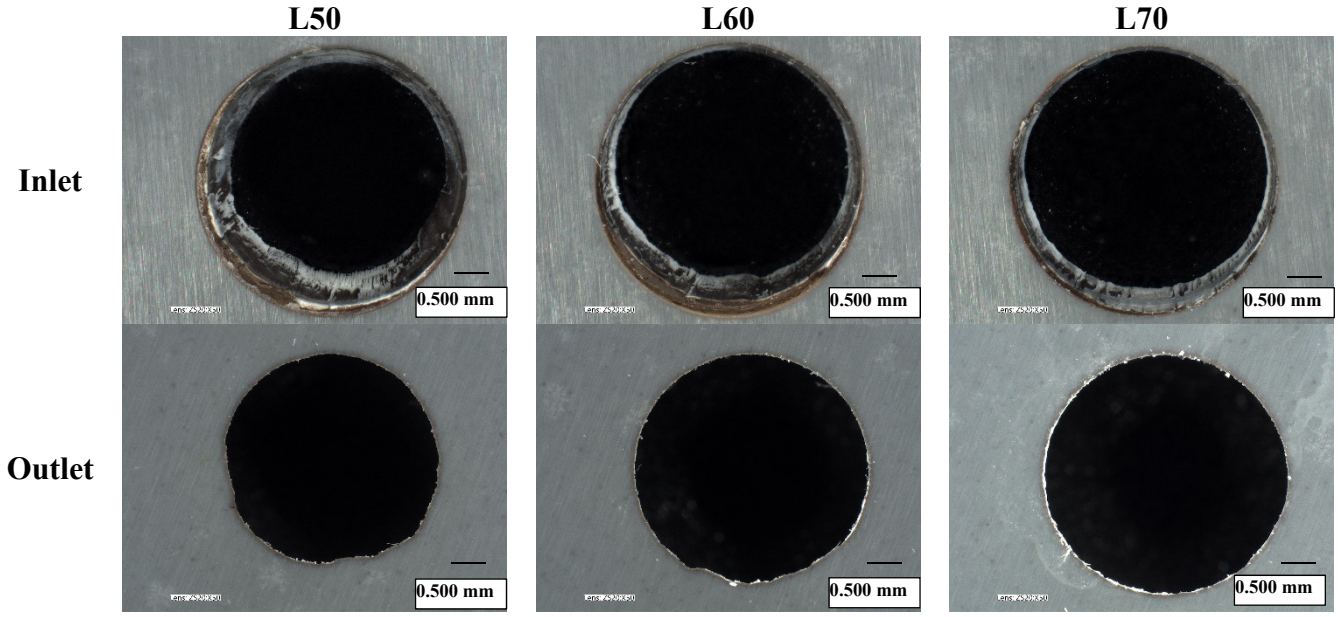

Figure 3: Digital microcopy of the L50, L60, and L70 hole inlet and outlets. Drilled at 0.15 mm hatch spacing. Measured using ZS20 Lens, Magnification: 50x

Results and Discussion

Micrographs of the inlet and outlet of specimen L50, 60, and 70 are provided in Figure 3. It is observed that the inlet holes are circular, and the surface exhibits low roughness. Additionally, the holes exhibited a crescent-shaped shear lip towards the lower-left side of the drilled hole. This is attributed to the beam focal distance. The edges of the inlet holes are discolored and have breakage around. As reviewed from the outlet micrographs, the outlets appear to gradually increase in circularity, as well as the edges become smooth and uniform.

Quantitatively, dimensions of the inlet and outlet were obtained using the Keyence microscope, described in Table 4. The target diameter is 4 mm. The most accurate inlet and outlet diameter is measured in test L70 with a diameters of 3.988 and 3.671 mm respectively. as well as the largest outlet diameter. Qualitative and quantitatively test L60 and L70 exhibit the largest and the smallest

shear lip thickness at 0.272 and 0.123 mm respectively. Overall, it is observed as the % power increases the outlet holes become more circular and uniform, the diameters begin to increase.

Table 4: Drilled hole dimensions

Test	Inlet Diameter (mm)	Outlet Diameter (mm)	Shear Lip Thickness (mm)
L50	3.951	3.251	0.207
L60	3.981	3.583	0.272
L70	3.988	3.671	0.123
L75.5	3.941	3.659	0.322

The cylindricity, taper, and taper angle values of the holes are shown in Table 5. The objective for all three measures should be zero, the highest (i.e., worst) values are observed in L50. As the % power is increased, cylindricity, taper, and taper angle improve. The best conditions in the original test matrix are reflected in L70, where cylindricity is 0.317 mm, taper is 0.105 and taper angle is 3.02°.

Table 5: Taper and cylindricity values

Test	Cylindricity (mm)	Taper	Taper Angle (°)
L50	0.700	0.230	6.65
L60	0.398	0.133	3.80
L70	0.317	0.105	3.02
L75.5	0.282	0.094	2.69

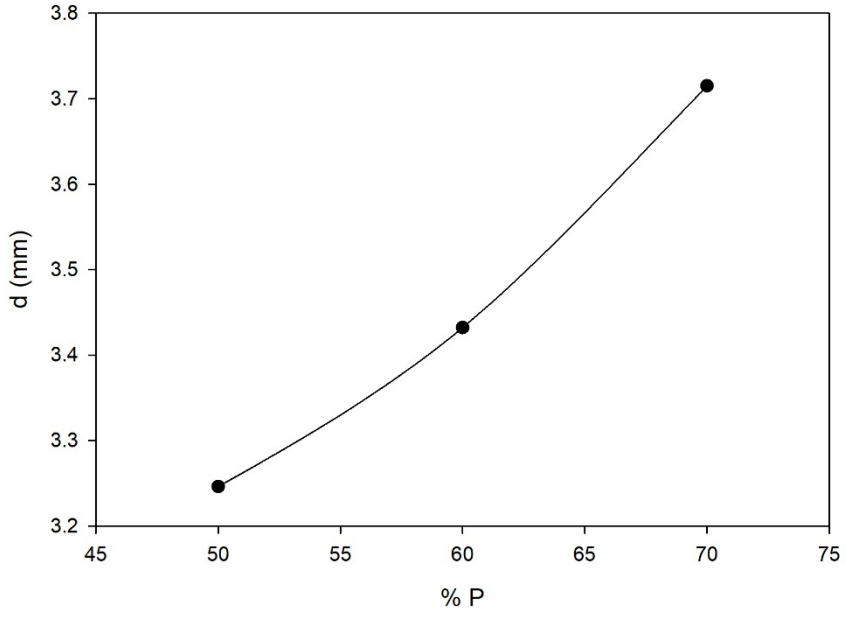

Figure 4: Diameter vs power at 0.015 mm

The outlet diameter vs % power was graphed in Figure 4. It is observed that as the % power increased the diameter increased as well. These results suggest that a target diameter of 4 mm was

possible, if the % power kept increasing. It was decided that the data would be fitted into a second order polynomial to obtain an equation that could solve for the target diameter as follows,

$$y = 0.0005x^2 - 0.0347x + 3.771 \quad (4)$$

Where, when y equals 4 mm, x is equated to 75.5%. This % power is hypothesized to have a outlet outcome of 4 mm as well as cylindricity, taper and taper angle measured to zero.

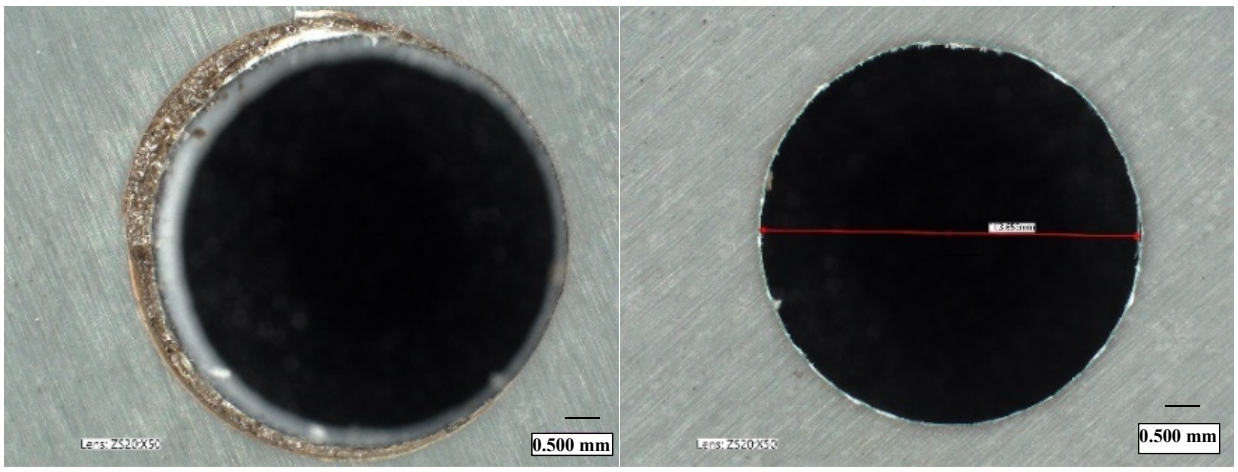

Figure 5: Digital microscopy of L75.5 inlet and outlet holes. Drilled at 0.015 mm hatch spacing. Measured using ZS20 Lens, Magnification: 50x

The inlet and outlet of the resulting secondary test are shown in Figure 5. A more prominent shear lip in the inlet hole is observed. Again, the inlet hole appears to have discoloration and breakage around the edge at the shear lip. The measurements for L75.5 are described in Tables 4 and 5. The inlet and the outlet hole measured 3.941 and 3.659 mm respectively. The outlet hole is uniform and circular and shows no effects form the drilling process. The shear lip present is greater than the previous three tests, this can be credited to the high energy. L75.5 showed improved cylindricity, taper and taper angle and are the best results from the matrix. Overall, L75.5 did not have the best outlet measurement but rescaling the geometry may help in obtaining the correct measurement.

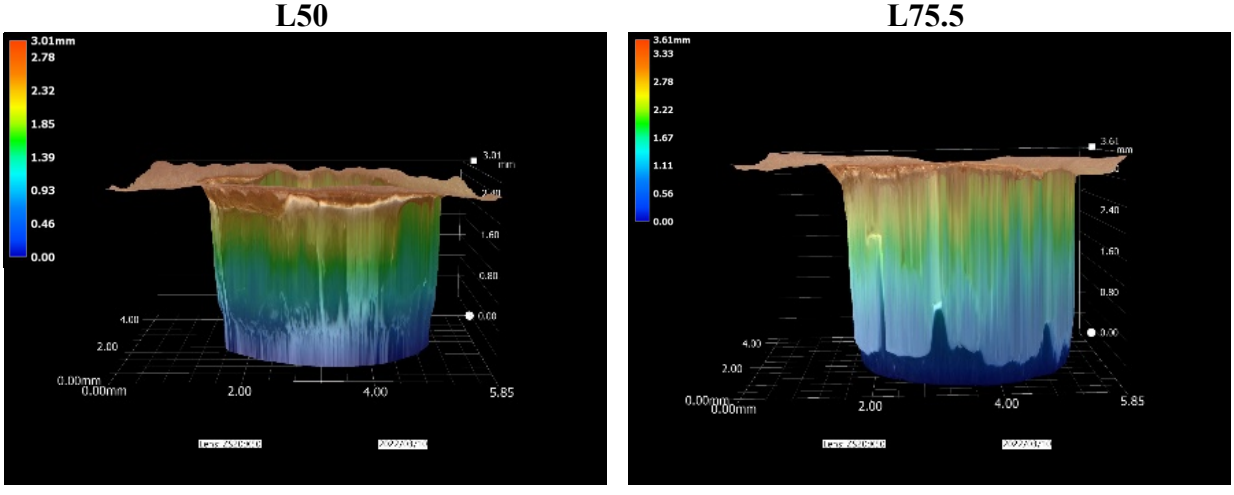

Figure 6: 3D mapping of tests L50 and L75.5. Measured using ZS20 Lens.

The 3D maps for the drilled holes with the largest (L50) and smallest (L75.5) taper are shown in Figure 6. In L50, it is observed that there is surface roughness, and the taper begins to develop at the bottom of the side view. In L75.5, although there was a slight taper measured, it is not evident in the images. Comparing the two, increasing the power helps in reducing the cylindricity, taper and taper angle.

Conclusion

The initial hypothesis that increasing the % power will yield better outlet holes, was proven true. Although with the increase of power and energy, the surface of the hole will endure discoloration and breakage. Additionally, the hypothesis for L75.5 was not accurate, while the equation provided a value for an outcome of 4 mm that was not the case. L70 produced a slightly greater outlet hole than L75.5, although L75.5 showed the best results in terms of cylindricity, taper and taper angle. Future work consists of polishing sample to remove shear lip, as well as rescale the size of the geometry to account for under sizing.

This work is funded by the Department of Energys Kansas City National Security Campus, operated by Honeywell Federal Manufacturing &Technologies, LLC, under contract number DE-NA0002839

References

1. Kim, S. H., Sohn, I.-B., & Jeong, S. (2009). Ablation characteristics of aluminum oxide and nitride ceramics during femtosecond laser micromachining. *Applied Surface Science*, *255*(24), 9717–9720. https://doi.org/10.1016/j.apsusc.2009.04.058
2. Atanasov, P. A., Eugenieva, E. D., & Nedialkov, N. N. (2001). Laser drilling of silicon nitride and alumina ceramics: A numerical and experimental study. *Journal of Applied Physics*, *89*(4), 2013–2016. https://doi.org/10.1063/1.1334367
3. Yang, J.-F., Ohji, T., & Niihara, K. (2000). Influence of Yttria–Alumina Content on Sintering Behavior and Microstructure of Silicon Nitride Ceramics. *Journal of the American Ceramic Society*, *83*(8), 2094–2096. https://doi.org/10.1111/j.1151-2916.2000.tb01520.x
4. *McMaster-Carr*. (n.d.). Retrieved March 21, 2022, from https://www.mcmaster.com/
5. V. Bharathi, A.R. Anilchandra, Shantanu Sanjay Sangam, S. Shreyas, Siddesh B. Shankar, A review on the challenges in machining of ceramics, Materials Today: Proceedings, Volume 46, Part 2, 2021, Pages 1451-1458, ISSN 2214-7853, https://doi.org/10.1016/j.matpr.2021.03.019.
6. Schulz, W., Eppelt, U., & Poprawe, R. (2013). Review on laser drilling I. Fundamentals, modeling, and simulation. *Journal of Laser Applications*, *25*. https://doi.org/10.2351/1.4773837
7. Wilson, J. and J. F. B. Hawkes. *Lasers: Principles and Applications.* Englewood Cliffs, NJ: Prentice-Hall, 1987. (TA1675.W55)
8. Soltani, B., Azarhoushang, B., & Zahedi, A. (2019). Laser ablation mechanism of silicon nitride with nanosecond and picosecond lasers. *Optics & Laser Technology*, *119*, 105644. https://doi.org/10.1016/j.optlastec.2019.105644
9. *Cylindricity | GD&T Basics*. (n.d.). Retrieved March 21, 2022, from https://www.gdandtbasics.com/cylindricity

10. Alkhalefah, H. (2020). Precise Drilling of Holes in Alumina Ceramic (Al2O3) by Rotary Ultrasonic Drilling and its Parameter Optimization using MOGA-II. *Materials*, *13*, 1059. https://doi.org/10.3390/ma13051059
11. *Process of Laser Machining*. (n.d.). Springerprofessional.De. Retrieved March 23, 2022, from https://www.springerprofessional.de/en/process-of-laser-machining/7437340